

Towards a physics-based relationship for crack growth under different loading modes

Amaral, Lucas; Alderliesten, René; Benedictus, Rinze

DOI

[10.1016/j.engfracmech.2018.04.017](https://doi.org/10.1016/j.engfracmech.2018.04.017)

Publication date

2018

Document Version

Final published version

Published in

Engineering Fracture Mechanics

Citation (APA)

Amaral, L., Alderliesten, R., & Benedictus, R. (2018). Towards a physics-based relationship for crack growth under different loading modes. *Engineering Fracture Mechanics*, 195, 222-241. <https://doi.org/10.1016/j.engfracmech.2018.04.017>

Important note

To cite this publication, please use the final published version (if applicable). Please check the document version above.

Copyright

Other than for strictly personal use, it is not permitted to download, forward or distribute the text or part of it, without the consent of the author(s) and/or copyright holder(s), unless the work is under an open content license such as Creative Commons.

Takedown policy

Please contact us and provide details if you believe this document breaches copyrights. We will remove access to the work immediately and investigate your claim.

Green Open Access added to TU Delft Institutional Repository

'You share, we take care!' – Taverne project

<https://www.openaccess.nl/en/you-share-we-take-care>

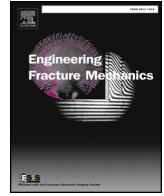
Otherwise as indicated in the copyright section: the publisher is the copyright holder of this work and the author uses the Dutch legislation to make this work public.



ELSEVIER

Contents lists available at ScienceDirect

Engineering Fracture Mechanics

journal homepage: www.elsevier.com/locate/engfracmech

Towards a physics-based relationship for crack growth under different loading modes



Lucas Amaral*, René Alderliesten, Rinze Benedictus

Structural Integrity & Composites Group, Faculty of Aerospace Engineering, Delft University of Technology, Kluyverweg 1, 2629HS Delft, The Netherlands

ABSTRACT

In an attempt to understand quasi-static delamination growth under mixed mode loading conditions from a physics-based perspective, this work first evaluated cracking in isotropic materials. The critical Strain Energy Density (SED) approach is adopted, because physically the onset of crack growth is expected to occur when the energy available near the crack tip reaches a critical value.

The main hypothesis of the present paper is that the critical SED for onset of crack growth is constant for a given material, and independent of the loading mode. The relationship derived from this hypothesis therefore relates the physical onset of crack growth and the angle at which that occurs for any opening mode through the SED.

To test this hypothesis, results from literature were taken and shear fracture tests on foam specimens were performed, which both were compared with the derived relationship. The excellent correlation demonstrated the validity of the physics-based relationship, which explains the observed differences between mode I and mode II fracture toughnesses and illustrates why concepts like the Stress Intensity Factor (SIF) alone are insufficient to explain the observations. The developed relationship allows to derive the mode II fracture toughness from mode I fracture toughness tests and the material's mechanical properties.

1. Introduction

Laminated composites are attractive for aerospace applications because of their high specific strength and stiffness [1]. However, their poor interlaminar strength makes them susceptible to delamination, which is the most observed damage mode in laminated composites [2,3]. The models currently used to assess delamination are not based on the physics of the problem [4]. Because of this lack of fundamental knowledge of the physics underlying delamination growth, composite structures in aircraft are overdesigned in order to safeguard the structural integrity of the airplane [5–7]. Such an overdesign hampers further weight reductions which could result in economic advantages to both aircraft manufacturer and operator [8]. Therefore, understanding the underlying physics of delamination growth is necessary for designing lighter load-bearing composite structures for aircraft.

Although delamination growth in composites has been widely studied in the past decades, there is a clear lack of understanding of its physics [4]. Quasi-static delaminations are usually characterized by means of the Strain Energy Release Rate (SERR), which is calculated just before the crack propagates and is referred to as the fracture toughness for the onset of delamination growth [9,10]. However, there is a gap between the macroscopic description of delamination through the SERR and the micromechanisms acting

* Corresponding author.

E-mail address: L.Amaral@tudelft.nl (L. Amaral).

Nomenclature		ENF	End-Notch Flexure
V	volume [m ³]	DCB	Double Cantilever Beam
$W_i(V)$	strain energy evaluated in an arbitrary volume [J]	MMB	Mixed-Mode Bending
S_i	critical strain energy density that causes the onset of crack growth [J/m ²]	<i>Greek symbols</i>	
G	shear modulus [GPa]	ν	Poisson's ratio
G_i	strain energy release rate [J/m ²]	θ_0	angle at which the strain energy density reaches a minimum value
E	elastic modulus [GPa]	<i>Subscripts</i>	
K_i	stress intensity factor [Pa m ^{1/2}]	crit	critical
P	potential energy per unit volume [J/m ³]	i = I, II, III, I/II	crack opening mode
U	strain energy per unit volume [J/m ³]	SED	value calculated using the SED approach
<i>Acronyms</i>		experimental	value obtained via experiments
SED	Strain Energy Density	ENF	value obtained via End-Notch Flexure specimens
SIF	Stress Intensity Factor		
SERR	Strain Energy Release Rate		

during fracture, as discussed elsewhere [10–12]. Thus, how does the fracture toughness connect with the physics underlying delamination growth? The micromechanisms and the macroscopic behaviour in delamination growth should be connected with a physics-based theory. This would enable a better understanding of this failure mode, which could lead to reliable design rules for the use of composites in aerospace structures.

In order to address this issue, studies available in literature have tried to connect the microscopic damage features with the macroscopic behaviour of damage growth. To this aim, these studies used the SERR and analyses of fracture surfaces to study the effects of resin toughness, resin layer thickness and loading mode in the resistance to delamination [13–18]. A commonly reported result in these studies is that the fracture toughness was observed to be higher for mode II delaminations than for mode I delaminations. The question to be asked at this point is: why? The analytical description of the stresses on the vicinity of the crack tip, such as criterion based on T-stresses [19–21], helps in understanding the problem, but was not able to answer this question yet.

Hibbs and Bradley suggested that the different micromechanisms acting in delamination growth were somehow connected to the difference in the measured fracture toughness for modes I and II. However, they claimed that there must be more to the story [14]. To the present day, a satisfactory answer to this question and the physics connecting delamination growth under different loading modes still have to be addressed.

1.1. Motivation

Properly designing composite aircraft structures, reaping all the advantages of their high specific strength and stiffness without overdesigning them, requires a better understanding of delamination. This includes understanding the physics behind delamination growth under different loading modes and how different loading modes relate.

To this aim, uncovering the relationship between the macroscopic resistance to crack propagation and the micromechanisms of delamination is of utmost importance [16].

In addition, once the physics of delamination and the connection between different loading modes are understood, the possibility of calculating fracture toughness data for different loading modes from material properties would dramatically reduce the number of tests necessary to characterize the fracture behaviour of the material. Consider the example in which a physics-based relationship between delamination under modes I and II is clear. Then, only with material properties and mode I fracture toughness data, one would be able to calculate mode II fracture toughness. This would reduce, or even eliminate, the necessity of mode II fracture toughness tests.

1.2. Objectives

This study aims to understand quasi-static crack growth from a physics-based perspective, uncovering the fundamental relationship that connects mode I and mode II fracture. This would enable mode II fracture data to be obtained from mode I fracture data and material properties. However, the reader should note that the aim of the present study is not yet to develop an engineering prediction model. Instead, the present study aims at testing the hypotheses presented in Section 2 in a broader fashion, using various data sets available in literature.

Therefore, the questions addressed in this paper are:

- What is the physics-based relationship between mode I and mode II fracture?
- The critical SERR is reported to be higher for mode II than for mode I delamination growth in most cases. What is the physical reason for this?

- How can one estimate mode II fracture toughness from material properties and mode I fracture toughness data?

1.3. Methodology

In order to answer the aforementioned questions, the present study scrutinizes quasi-static delamination growth under loading modes I and II. This is accomplished through an analytical description of the stresses and the strain energy concentrated around the crack tip for each case. The starting point of this paper is the analytical treatment of a simpler case, considering mode I and mode II fracture of isotropic, linear elastic, brittle materials. This analysis is followed by the analytical consideration of stresses and strain energy around the crack tip of approximately brittle, orthotropic, linear elastic composite laminates. In order to shed light on the complex mechanisms of mode II delamination growth, rail shear tests were performed in PVC foam specimens, and a qualitative analysis of the delamination process is presented. Finally, the relationship between mode I and mode II fracture is discussed.

2. Hypotheses

2.1. Fracture and energy

Fracture, which is decohesion of material, is controlled by energy [22]. When a structure is loaded, potential strain energy is stored in that structure. For a given material, once the strain energy at a certain point of the body reaches a critical value, the onset of fracture occurs. Therefore, fracture is limited by a critical strain energy at which decohesion occurs for a certain material [23,24]. The critical strain energy for the onset of fracture might be reached by shear stresses, normal stresses or combinations thereof. Therefore, this critical strain energy for the onset of fracture is hypothesized to be independent of the loading mode.

In addition, when analysing crack propagation, instead of considering the stresses at the crack tip, the stresses distributed over a small area around the crack tip will be considered of influence to fracture. This is based on the concept presented in the work of Neuber [25,26] and also developed later by Lazzarin and colleagues [27,28], in which stresses distributed around the crack tip are said to provide support to the highly stressed area at the tip of the crack. Besides, the stress distribution ahead of the crack tip, which changes with the loading mode, was shown to determine the damage mechanisms acting on fracture and observed on the fracture surfaces for ply delaminations [7,14,16]. Therefore, in order to account for the damage mechanisms when characterizing the energy dissipated in fracture, the stress distribution around the crack tip must be considered. These hypotheses are thoroughly discussed in further sections of the present work.

2.2. Saint-Venant’s principle

Following Saint-Venant’s principle, only the strain energy stored in the direct vicinity of the crack tip determines the crack increment. The effect of the strain energy stored in areas far away from the crack tip is considered negligible for crack growth.

Therefore, consider the two cracked bodies of the same material, illustrated in Fig. 1(a) and (b), loaded under modes I and II, respectively. Now, consider the same arbitrary volume V is used to evaluate the strain energy that causes fracture for both modes I and II, as illustrated in Fig. 1. The strain energy in this arbitrary volume V due to mode I loading is $W_I(V)$. Similarly, the strain energy in the volume V due to mode II loading is $W_{II}(V)$. Taking into consideration the hypothesis of Section 2.1, once the strain energy at a certain point of the body reaches a critical value, the onset of fracture occurs, independently of the loading mode. This is equivalent to saying that $W_I(V) = W_{II}(V)$ at the moment of fracture onset. Logically, if the volume V at which the strain energy is evaluated for both cases in Fig. 1 is the same, then the critical strain energy per volume that causes the onset of mode I crack growth, S_I , is equal to

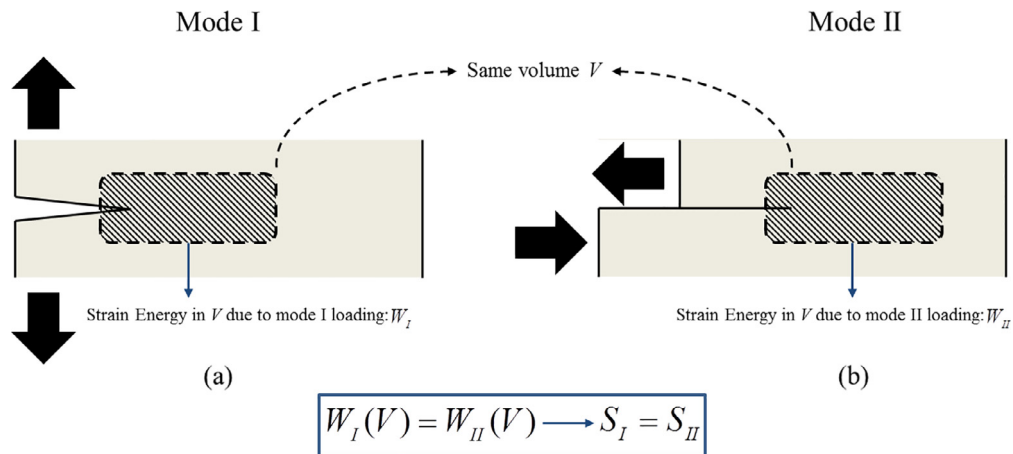


Fig. 1. (a) Cracked body under mode I loading; (b) cracked body under mode II loading. Both cracked bodies are from the same material. The strain energy density S that causes fracture is the same for both loading modes.

the critical strain energy per volume that causes the onset of mode II crack growth, S_{II} . Therefore, because of the hypothesis that the strain energy for the onset of fracture is independent of the loading mode, and because the same arbitrary region in the vicinity of the crack tip is being used to compare fracture under any loading mode, the shape and size of this region do not need to be formally defined.

2.3. Pure mode I fracture

Energy dissipation due to other mechanisms besides crack growth such as friction, contact with load introduction structures, fixture compliance and energy dissipation in the process zone ahead of the main crack tip is considered to be small for the onset of mode I fracture. Therefore, the Stress Intensity Factor (SIF) and, consequently, the SERR for the onset of mode I crack growth are considered to include only the effects of energy dissipated in crack increment.

3. Rail shear tests

In order to understand crack growth under modes I and II and their relationship, the understanding of the formation of a process zone ahead of the crack tip is necessary [7,12]. According to literature [12,15,16,29,30], the formation of microcracks in the process zone ahead of the main crack tip and the energy they dissipate on delamination growth are detrimental for mode II crack propagation. Mode I process zones are smaller than mode II process zones, and their effect can be regarded as negligible for delamination extension [15,16].

In order to properly observe, at real time, the formation of this process zone, in-situ mode II delamination tests would be necessary. However, the scale and inhomogeneity of mode II delamination makes it very hard to actually observe the phenomenon. Without actual observation the formation of a process zone, common delamination experimental campaigns would hardly shed any light on process zone formation and onset of mode II cracking. Thus, in an attempt to shed light onto the problem of damage mechanisms in mode II delaminations, Greenhalgh and Rogers et al. [31,32] performed rail shear tests in PVC foam specimens. The shear tested PVC foam yielded a macroscopic fracture surface with morphologies similar to the ones encountered at the microscale in mode II delamination of composites. With the advantage of avoiding the use of a Scanning Electron Microscope (SEM) and enabling naked eye observations of mode II damage mechanisms and process zone formation, the rail shear tests were deemed as a good qualitative representation of mode II delaminations.

Therefore, to better understand mode II process zone formation and support the analyses of the present work, four Divinycell® H-200 PVC foam specimens, identical to the ones used in [31–33], were tested in a Rail Shear test fixture. The properties of Divinycell® H-200 PVC foam are given in the manufacturer’s technical manual [34] and displayed in Table 1.

The tests followed the guidelines given by ASTM C-273 [35] and the dimensions of the specimens are shown in Fig. 2. The chosen cross-section in Fig. 2(b) and pre-crack length of 70 mm were the ones that produced cusp-like features on the fracture surfaces of the foam. Specimens with this cross-section were observed to represent mode II delamination fracture surfaces better than the other cross-section geometries proposed in literature, enabling a qualitative investigation of mode II process zone development and cusp formation [31,32].

All tests were performed in a hydraulic machine equipped with a 60 kN load cell, using a loading rate of 3 mm/min. A camera was positioned alongside the specimens in order to monitor process zone formation and crack propagation.

4. The critical strain energy density

4.1. Isotropic materials

Following the hypotheses that fracture is controlled by energy and that the crack advances when the strain energy around the crack tip reaches a critical value, the strain energy distribution around the crack tip must be determined. To this aim, consider a structure made of an isotropic, linear elastic material under a general three-dimensional stress state. The strain energy stored in an element of volume dV is given by Eq. (1), where $G = E/2(1 + \nu)$ is the shear modulus, E is the elastic modulus and ν is Poisson’s ratio [36].

$$dW = \left[\frac{1}{2E}(\sigma_x^2 + \sigma_y^2 + \sigma_z^2) - \frac{\nu}{E}(\sigma_x\sigma_y + \sigma_y\sigma_z + \sigma_z\sigma_x) + \frac{1}{2G}(\tau_{xy}^2 + \tau_{xz}^2 + \tau_{yz}^2) \right] dV \tag{1}$$

Suppose that this structure has a through-crack that extends in the xz -plane, illustrated in Fig. 3. The stresses around the crack tip were described by Irwin [37] and are given by

Table 1
Material properties for Divinycell® H-200 PVC foam [34].

Nominal density	200 kg/m ³
Tensile modulus	250 MPa
Shear modulus	85 MPa

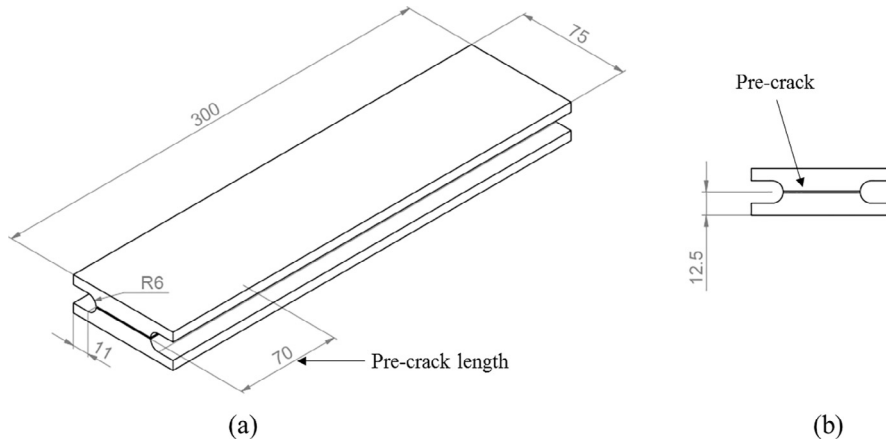


Fig. 2. (a) Dimensions of the Divynycell H-200 PVC foam specimen; (b) location of the 70 mm long pre-crack created with a saw-cut. All dimensions are in millimetres.

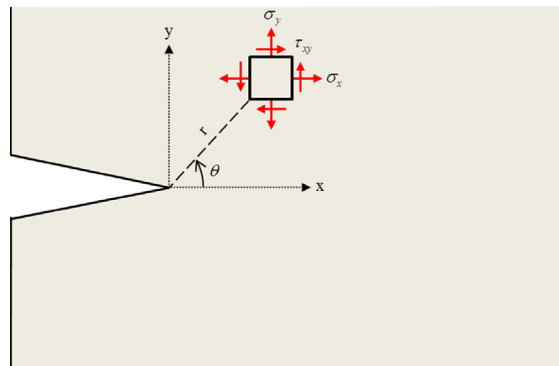


Fig. 3. Stresses around the tip of a through crack extending on the *xy*-plane.

$$\begin{aligned}
 \sigma_x &= \frac{K_I}{\sqrt{2\pi r}} \cos(\theta/2) [1 - \sin(\theta/2) \sin(3\theta/2)] - \frac{K_{II}}{\sqrt{2\pi r}} \sin(\theta/2) [2 + \cos(\theta/2) \cos(3\theta/2)] \\
 \sigma_y &= \frac{K_I}{\sqrt{2\pi r}} \cos(\theta/2) [1 + \sin(\theta/2) \sin(3\theta/2)] + \frac{K_{II}}{\sqrt{2\pi r}} \sin(\theta/2) \cos(\theta/2) \cos(3\theta/2) \\
 \sigma_z &= 2\nu \frac{K_I}{\sqrt{2\pi r}} \cos(\theta/2) - 2\nu \frac{K_{II}}{\sqrt{2\pi r}} \sin(\theta/2) \\
 \tau_{xy} &= \frac{K_I}{\sqrt{2\pi r}} \cos(\theta/2) \sin(\theta/2) \cos(3\theta/2) + \frac{K_{II}}{\sqrt{2\pi r}} \cos(\theta/2) [1 - \sin(\theta/2) \sin(3\theta/2)]
 \end{aligned} \tag{2}$$

with higher order terms in *r* neglected. *K_i* stands for the Stress Intensity Factor (SIF), being *i* the loading mode (I, II or III).

Although the case described is of a crack extension in the *xz*-plane, the reader should note that any crack is locally under plane strain conditions [37]. Therefore, a stress in the *z*-direction is considered in this analysis. The reader should be aware that, according to the fracture problem assessed, the stresses presented in Eq. (2) can be modified to account for a 3D stress state and mode III crack opening.

Substituting the stresses given by Eq. (2) in Eq. (1), one obtains the strain energy stored in a volume element *dV* at any point around the crack tip, which is

$$\frac{dW}{dV} = \frac{1}{\pi r} (a_{11} K_I^2 + 2a_{12} K_I K_{II} + a_{22} K_{II}^2) \tag{3}$$

The intensity of the strain energy density field around the crack tip is, then, given by

$$S = a_{11} K_I^2 + 2a_{12} K_I K_{II} + a_{22} K_{II}^2 \tag{4}$$

where the coefficients *a₁₁*, *a₁₂* and *a₂₂*, and the complete deduction of these equations are given in Appendix A. The concept and the term *S*, known as Strain Energy Density (SED), were first introduced by Sih and colleagues in a series of investigations on fracture mechanics of brittle materials [23,24,38].

For the cases of pure mode I and pure mode II loading, the SED is given by respectively

$$S_I = \frac{K_I^2}{16G} [(3-4\nu-\cos\theta)(1 + \cos\theta)] \tag{5}$$

$$S_{II} = \frac{K_{II}^2}{16G} [4(1-\nu)(1-\cos\theta) + (1 + \cos\theta)(3\cos\theta-1)] \tag{6}$$

4.2. Orthotropic materials

Consider, once more, a structure with a through-crack that extends on the xz -plane, shown in Fig. 3. This time the structure is made of a linear elastic, orthotropic material. In this case, the strain energy stored in a volume element dV is

$$\frac{dW}{dV} = \frac{1}{2} \left[\frac{\sigma_x^2}{E_x} + \frac{\sigma_y^2}{E_y} + \frac{\sigma_z^2}{E_z} + \frac{\tau_{xy}^2}{G_{xy}} \right] - \frac{\nu_{xy}\sigma_x\sigma_y}{E_x} - \frac{\nu_{xz}\sigma_x\sigma_z}{E_x} - \frac{\nu_{yz}\sigma_y\sigma_z}{E_y} \tag{7}$$

The stresses around the crack tip of orthotropic bodies were described by Sih et al. [38] and are given in the expressions in

$$\begin{aligned} \sigma_x &= \frac{K_I}{\sqrt{2\pi r}} A_I + \frac{K_{II}}{\sqrt{2\pi r}} A_{II} \\ \sigma_y &= \frac{K_I}{\sqrt{2\pi r}} B_I + \frac{K_{II}}{\sqrt{2\pi r}} B_{II} \\ \sigma_z &= \left(\frac{K_I}{\sqrt{2\pi r}} A_I + \frac{K_{II}}{\sqrt{2\pi r}} A_{II} \right) \frac{\nu_{xz} E_z}{E_x} + \left(\frac{K_I}{\sqrt{2\pi r}} B_I + \frac{K_{II}}{\sqrt{2\pi r}} B_{II} \right) \frac{\nu_{yz} E_z}{E_y} \\ \tau_{xy} &= \frac{K_I}{\sqrt{2\pi r}} C_I + \frac{K_{II}}{\sqrt{2\pi r}} C_{II} \end{aligned} \tag{8}$$

The coefficients A_i , B_i and C_i , for $i = I$ and II , are given in Appendix A. The strain energy stored in a volume element dV becomes

$$\frac{dW}{dV} = \frac{1}{2\pi r} (K_I^2 D_1 + K_{II}^2 D_2 + K_I K_{II} D_3) \tag{9}$$

where the SED is $S = K_I^2 D_1 + K_{II}^2 D_2 + K_I K_{II} D_3$ and the coefficients D_i , for $i = 1, 2$ and 3 , are described in Appendix A.

A useful application is to use Eq. (9) to determine the critical SED for delamination growth in orthotropic composite structures. The reader should note, however, that this consists of an approximation. The expressions of the stresses around the crack tip in Eq. (8) were developed for homogeneous bodies. However, composites are obviously not homogeneous. Hence, the reader should be aware that Eq. (8) does not give exact solutions for stresses around the crack tip of an orthotropic composite structure. Furthermore, the calculation of SIF's for composites is not straightforward. Therefore, writing Eq. (9) in terms of the SERR is useful, once the SERR is easier to be determined for composites than the SIF. For orthotropic materials under plane stress the SERR for both mode I and mode II loading are [39]

$$\begin{aligned} G_I &= F_I K_I^2 \\ G_{II} &= F_{II} K_{II}^2 \end{aligned} \tag{10}$$

where

$$F_I = \sqrt{\frac{A_{11} A_{22}}{2}} \left[\sqrt{\frac{A_{22}}{A_{11}}} + \frac{2A_{12} + A_{66}}{2A_{11}} \right]^{1/2} \tag{11}$$

$$F_{II} = \frac{A_{11}}{\sqrt{2}} \left[\sqrt{\frac{A_{22}}{A_{11}}} + \frac{2A_{12} + A_{66}}{2A_{11}} \right]^{1/2} \tag{12}$$

And the coefficients A_{11} , A_{12} , A_{22} and A_{66} are given in the Appendix.

4.3. Strain energy density and potential energy in the system

The relationship between the potential energy that goes into the structure and the strain energy density has been discussed by Sih [23]. However, for convenience of the reader, this relationship is summarized in the present section.

Consider a structured loaded under its linear elastic limits. The potential energy per unit volume of an element located at a distance r from the crack tip is P , while the strain energy per unit volume is $U = dW/dV$. If the cracked body is subjected to displacement controlled loading, the strain energy is equal to the negative of the potential energy, such that $P = -U$. However, as $U = dW/dV = S/r$, then

$$P = \frac{-S}{r} \tag{13}$$

Crack propagation is assumed to occur in the direction where the potential energy density is maximum, which means

$$\begin{aligned} \frac{\partial P}{\partial \theta} &= 0, \theta = \theta_0 \\ \frac{\partial^2 P}{\partial \theta^2} &< 0, \theta = \theta_0 \end{aligned} \tag{14}$$

Rewriting Eq. (14) in terms of the SED, one obtains a condition for the critical SED, i.e., the SED at which the onset of crack propagation occurs:

$$\begin{aligned} \frac{\partial S}{\partial \theta} &= 0, \theta = \theta_0 \\ \frac{\partial^2 S}{\partial \theta^2} &> 0, \theta = \theta_0 \end{aligned} \tag{15}$$

Applying the conditions expressed in Eq. (15) to Eq. (5), the SED is shown to achieve a minimum value at $\theta_0 = 0^\circ$ for a linear elastic, isotropic material under pure mode I loading. In this case, the critical SED is

$$S_{Icr} = \frac{K_{Icr}^2 (1-2\nu)}{4G} \tag{16}$$

Similarly, applying the conditions in Eq. (15) to Eq. (6), the SED is shown to achieve a minimum value at $\cos(\theta_0) = (1-2\nu)/(4G)$ for a linear elastic, isotropic material under pure mode II loading. The critical SED is, then:

$$S_{IIcr} = \frac{K_{IIcr}^2 [8(1-\nu)-4\nu^2]}{48G} \tag{17}$$

5. Results and discussion

5.1. Brittle isotropic materials

Following the discussion in Section 5.2 of the present work, fracture is controlled by energy. When the SED around the crack tip reaches a critical value, crack growth occurs. From the perspective of the material, the energy necessary for the onset of crack growth is independent of the loading mode. Therefore, one can state that the critical SED necessary for the onset of a pure mode I crack is the same as the critical SED necessary for the onset of a pure mode II crack:

$$S_{Icr} = S_{IIcr} \tag{18}$$

Eq. (18) presents the relationship between loading modes I and II. Furthermore, using Eqs. (16)–(18), one obtains a way of determining the mode II SIF from mode I SIF and material data. This concept of determining mode II fracture toughness from mode I fracture toughness and material data, which is a direct consequence of Eq. (18), will be referred to, from now on, as the critical SED approach. The reader should note, however, that

$$\frac{K_{IIcr}}{K_{Icr}} = \left(\frac{12(1-2\nu)}{8-8\nu-4\nu^2} \right)^{1/2} \tag{19}$$

is limited to linear elastic, brittle, isotropic materials.

Plotting Eq. (19) enables to visualize how the critical mode I and mode II SIFs relate according to Poisson’s ratio, as given in Fig. 4. Eq. (19) shows how pure mode I and pure mode II SIFs relate for linear elastic, brittle, isotropic materials. In order to test whether this relationship can indeed be used for predicting the pure mode II critical SIF or not, Eq. (19) is applied to different materials reported in literature in the following sections of the present work.

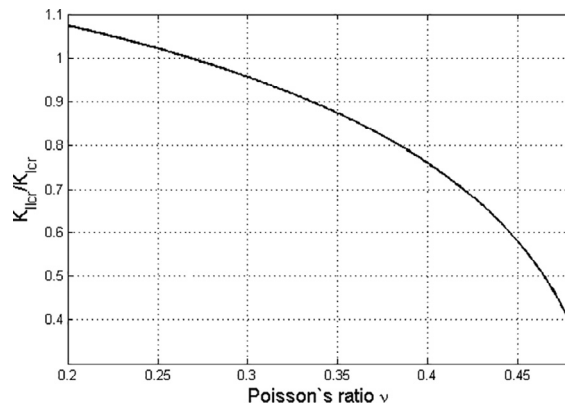


Fig. 4. Theoretical relationship between K_{IIcr}/K_{Icr} and Poisson’s ratio – modes I and II SIF for brittle, linear elastic, isotropic materials.

5.1.1. Plexiglass

Erdogan et al. [40,41] performed a series of fracture mechanics tests on Plexiglass, a brittle, isotropic, linear elastic material. In their experiments, the authors obtained a Poisson’s coefficient of $\nu = 0.3447 \pm 0.0254$ and a ratio between the critical SIFs for fracture under pure modes I and II of

$$\left(\frac{K_{IIcr}}{K_{Icr}}\right)_{\text{experiment}} = 0.89 \pm 0.12 \tag{20}$$

Using only Poisson’s coefficient for Plexiglass in Eq. (19), one obtains through the critical SED approach that

$$\left(\frac{K_{IIcr}}{K_{Icr}}\right)_{\text{SED}} = 0.88 \pm 0.09 \tag{21}$$

The prediction of Eq. (21) is in very good agreement with the experimental result from Erdogan et al. in Eq. (20). This suggests that, for Plexiglass, the strain energy density distributed around the crack tip controls fracture, and the critical strain energy density for fracture is, indeed, independent of the loading mode.

5.1.2. Rock samples

In order to test the validity of Eq. (19) for other brittle materials, fracture data from rock samples were obtained from literature and analysed using the critical SED approach. The comparison between experimental data and the prediction via SED is listed in Table 2. The Poisson’s ratio and $(K_{IIcr}/K_{Icr})_{\text{experiment}}$ were obtained from experiments described in literature. $(K_{IIcr}/K_{Icr})_{\text{SED}}$ is the prediction obtained through Eq. (19).

The prediction of $(K_{IIcr}/K_{Icr})_{\text{SED}}$ seems to be in good agreement with the experimental data obtained from literature. Therefore, one would be able to calculate with good accuracy pure mode II fracture toughness possessing only pure mode I fracture toughness and material data. However, the reader should note that there are limitations when using data from rock samples, once it is notoriously difficult to subject rock specimens to pure traction or shear [46,48].

In addition, Backers observed a significant variation on the experimentally obtained values of $(K_{IIcr}/K_{Icr})_{\text{experiment}}$ described in literature [48]. An example of this variation is shown in Table 3. The experimental values of pure mode I and II fracture toughness can vary, among other things, with the rock subtype, grain size, moisture content and type of test method used. The same rock can present different material behaviour, such as plasticity, in case these properties change [46]. A simple example is Poisson’s ratio for Indiana Limestone, which is assumed by Ingraffea [43] to be equal to $\nu = 0.20$, while Daneshy [44] used $\nu = 0.32$. In the results presented in Table 2, $\nu = 0.32$ was used for being the value of Poisson’s ratio that yielded the worst prediction in comparison with the experimental data, in order to show the limitations of the results. This shows that, even with a significant variation in ν , the worst prediction for Indiana Limestone through the SED approach still yields a result that is in relatively good agreement with the experimental data. Furthermore, the critical SED approach developed here is shown to be of valuable use to linear elastic, isotropic, brittle materials. Therefore, scientists and engineers must analyse to what extent the critical SED can be used to characterize the material in question.

5.2. Orthotropic composite laminates

The critical SED approach can be used in order to study delamination growth in orthotropic laminates. Suppose a delamination under pure mode I loading in a linear elastic, orthotropic laminate. The critical SED is given by

$$S_{Icr} = \frac{G_{Icr}}{F_I} D_1(\theta_{0I}) \tag{22}$$

where D_1 has a minimum value at θ_{0I} and is given in Appendix A, similarly to F_I . G_{Icr} is the critical SERR for the onset of mode I delamination. The latter is typically obtained via a Double Cantilever Beam (DCB) test, described by an ASTM standard [9]. Similarly, for pure mode II loading,

$$S_{IIcr} = \frac{G_{IIcr}}{F_{II}} D_2(\theta_{0II}) \tag{23}$$

Therefore, applying Eqs. (22) and (23) to the condition in Eq. (18), the critical SED approach can be used to characterize the

Table 2
Comparison of pure modes I and II fracture toughness obtained from experiments described in literature with fracture toughness predicted by the SED.

Rock	ν	$(K_{IIcr}/K_{Icr})_{\text{experiment}}$	$(K_{IIcr}/K_{Icr})_{\text{SED}}$	References for experimental data
Westerly Granite	0.20	≈ 1.10	1.07	[42,43]
Indiana Limestone	0.32	≈ 1.10	0.93	[43,44]
Dry snow	0.20	1.10	1.07	[45–47]

Table 3

Variation on the experimental results of pure modes I and II fracture toughness found in literature [48]

Rock	K_{Icr} (MPa m) ^{1/2}	K_{IIcr} (MPa m) ^{1/2}	$(K_{IIcr}/K_{Icr})_{\text{experiment}}$
Sandstone	From 0.67 to 2.56	From 0.32 to 4.95	From 0.48 to 1.93
Marble	From 0.46 to 2.25	From 3.33 to 6.36	From 2.83 to 7.23

critical SED to fracture in delamination growth. The critical SERR for the onset of mode II delamination can be estimated from material properties and pure mode I delamination tests:

$$G_{IIcr} = G_{Icr} \frac{F_{II} D_1(\theta_{0I})}{F_I D_2(\theta_{0II})} \tag{24}$$

5.2.1. HTA/6376C carbon/epoxy composite

In order to test the critical SED approach in delamination growth of orthotropic composite laminates, data from different sources in literature were obtained and the estimated G_{IIcr} was compared to the ones obtained via experiments. Usually, the mode II critical SERR was obtained testing End Notch Flexure specimens, recently described by an ASTM standard [49].

The first composite system analysed was HTA/6376C carbon/epoxy used by Asp et al. in two different studies [50,51]. The material data given in literature is described below. The specimen lay-up was (012//(\pm 5/04)S). The sign “//” refers to the plane of the artificial delamination. According to Asp et al., the offaxis angle was introduced to reduce fibre bridging at delamination growth. The specific lay-up was chosen to allow a small off-axis interface angle, while keeping the specimen properties close to those of a unidirectional specimen [51] (see Table 4).

Solving Eq. (24) numerically for the material properties and G_{Icr} given above, the SERR for the onset of pure mode II crack growth is estimated, as well as the angles in which the functions D_1 and D_2 are minimum. The angle in which the function D_1 reaches its minimum is the angle predicted for the first crack propagation under a pure mode I delamination. Similarly, the angle in which the function D_2 reaches its minimum is the angle predicted for the first crack propagation under a pure mode II delamination. The results, obtained by numerically solving Eq. (24) and finding the angles for which D_1 and D_2 are minimum, are shown in Table 5.

In order to assess the accuracy of the estimations in Table 5, experimentally obtained data is used for comparison. The critical SERR estimated for the onset of mode II crack growth is approximately 23% of the value obtained in ENF experiments performed by Asp and colleagues [50,51]. This difference in the critical SERR is observed because the value of SERR obtained via ENF experiments does not refer to the onset of crack growth.

What is the SERR obtained via ENF tests giving us?

In mode II delamination growth, a process zone develops with the formation of cusps, striations and microcracks ahead of the crack tip until coalescence is reached and crack growth can be observed from the sides of the specimen [12,16,29,30,51,52]. Only when coalescence is reached, a drop in the load is observed in the load-displacement history. The maximum load is then used to calculate the value of the critical SERR [12]. This is illustrated in Fig. 5.

Fig. 5(a) illustrates that the first crack growth occurs when the load is still below the maximum, and no load drop is observed. This first crack growth cannot be observed by naked eye observation of the sides of the specimen. This is followed by cusps formation (Fig. 5(b)) and their subsequent coalescence (Fig. 5(c)). Then, a drop in the load is observed. Therefore, the onset of mode II delamination occurs before the specimen reaches its mode II critical SERR determined via ENF tests [12].

The mode I SERR obtained via DCB tests refers to the onset of mode I crack growth, while the mode II SERR obtained via ENF tests refers to the coalescence of microcracks ahead of the crack tip. This is the reason why mode II SERR is usually reported to be higher than mode I SERR. The critical SERR obtained via ENF specimens, which is calculated only after coalescence has happened (Fig. 5(c)), is from now on referred to as $(G_{IIcr})_{ENF}$. Meanwhile, the critical SERR for the onset of mode II crack growth, determined with the critical SED approach and shown in Fig. 5(a), is referred to as $(G_{IIcr})_{SED}$. Therefore, if one considers the actual onset of crack growth for modes I and II, i.e., the first cracking, the onset of a mode I crack growth, at $G_{Icr} = 219.55 \text{ J/m}^2$, occurs at a higher SERR than the onset of mode II crack growth, at $(G_{IIcr})_{SED} = 201.75 \text{ J/m}^2$. However, why would the first cracks appear at a lower SERR for mode II than for mode I?

The answer to the question above lies in the characteristics of the stress distributions in the vicinity of the crack tip for each loading mode. This question is addressed in detail in Section 5.3 of the present work.

For now, another question will be discussed first: how to verify that the onset of mode II crack growth actually occurs at $(G_{IIcr})_{SED}$ and not at $(G_{IIcr})_{ENF}$? Asp and colleagues did verify that, indeed, the onset of delamination growth occurs before $(G_{IIcr})_{ENF}$. They

Table 4

Material data for HTA/6376C carbon/epoxy system.

Young’s Modulus	$E_x = 146 \text{ GPa}$ and $E_y = E_z = 10.5 \text{ GPa}$
Shear Modulus	$G_{xy} = G_{xz} = 5.25 \text{ GPa}$ and $G_{yz} = 3.48 \text{ GPa}$
Poisson’s ratio	$\nu_{xy} = \nu_{xz} = 0.30$ and $\nu_{yz} = 0.51$
SERR	$G_{Icr} = 219.55 \text{ J/m}^2$ and $G_{IIcr} = 883.10 \text{ J/m}^2$

Table 5
Estimation of parameters for the onset of pure modes I and II delaminations.

Angle for minimum D_1	Angle for minimum D_2	Estimated G_{IIcr}
-46.57°	-80.74°	201.75 J/m^2

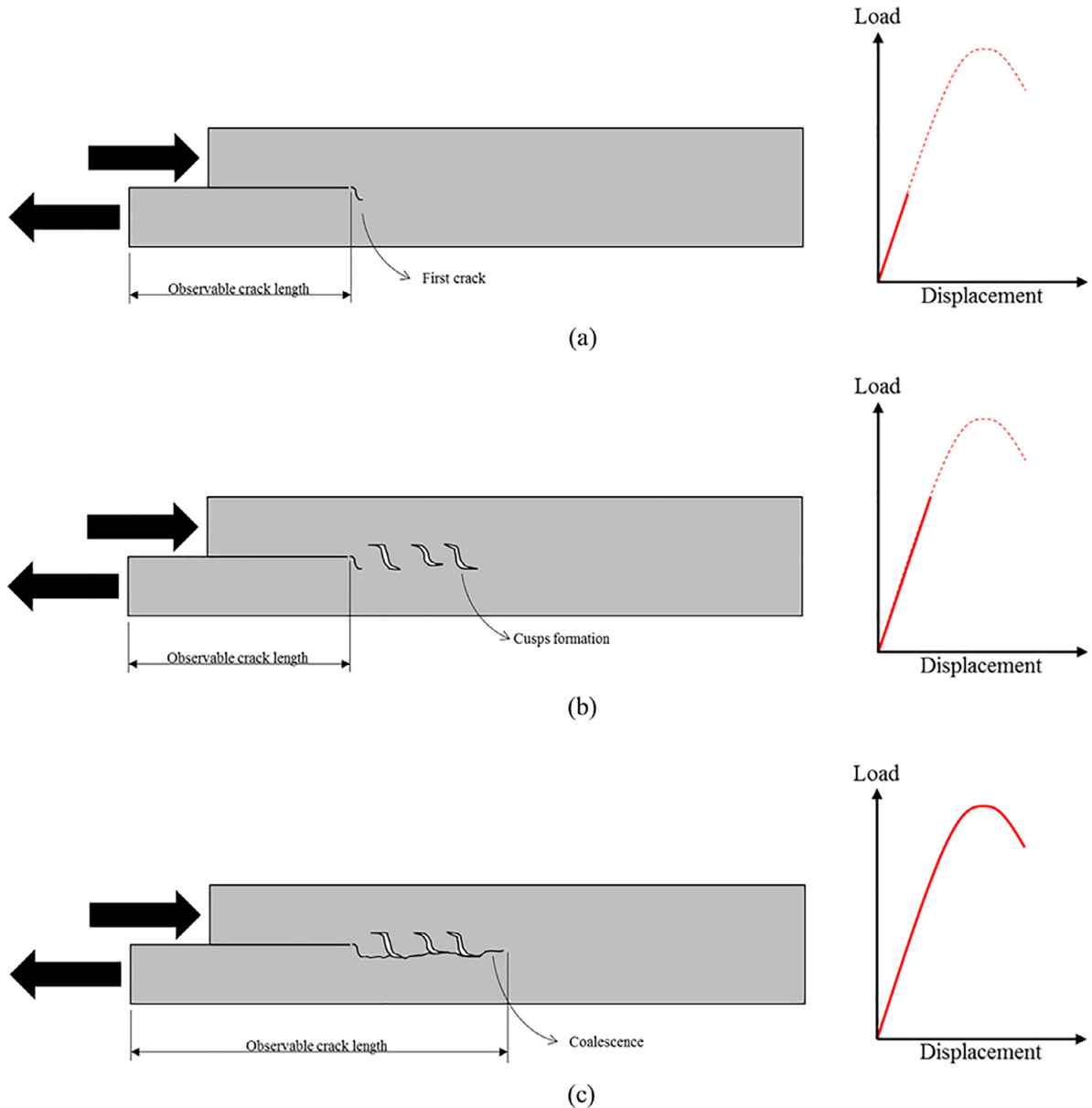


Fig. 5. Process zone formation in mode II delaminations. (a) First crack occurs before maximum load is achieved, followed by (b) cusps formation and (c) coalescence.

observed the sides of quasi-statically loaded ENF specimens in a SEM. Cracks ahead of the main crack tip were observed even in specimens loaded only until 50% of $(G_{IIcr})_{ENF}$ [51]. One of the images Asp et al. obtained in the SEM is reproduced in Fig. 6 for convenience of the reader.

These cracks ahead of the main crack tip were not observed when the specimen was loaded until 25% of $(G_{IIcr})_{ENF}$, which is approximately the threshold for the onset of crack propagation determined by means of the critical SED in Eq. (23). Asp and colleagues did not observe, however, the crack tip itself, and could not tell whether the first crack had already grown when the specimen was loaded up to 25% of $(G_{IIcr})_{ENF}$. Thus, the prediction of a first crack occurring in mode II delaminations at $(G_{IIcr})_{SED}$ is

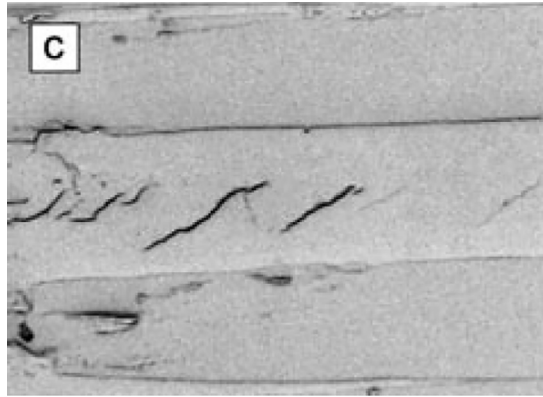


Fig. 6. Cracks ahead of the main crack tip in an ENF specimen loaded up to 50% of $(G_{Icr})_{ENF}$ (reproduced from [51]).

plausible according to data from literature. However, the actual verification of it would require in-situ mode II delamination tests.

Regarding the angles of the first crack predicted for the onset of both pure mode I and pure mode II delaminations, correlations with experimental data can also be drawn. For the onset of pure mode I delamination growth, the angle predicted for the first crack to grow was of -46.57° . Khan et al. [53] performed quasi-static mode I delamination tests on DCB specimens of a similar carbon/epoxy composite system inside of a SEM. They observed that the cracks did not propagate straight. Instead, they grew in angle with the x -axis, such that the crack touched the upper or lower fibres of adjacent layers, similarly to the angle of -46.57° predicted by the critical SED approach. This behaviour was also observed by Hibbs and colleagues during in-situ mode I tests [14]. Therefore, the prediction of the angle of the first crack for mode I delaminations seems to be in agreement with literature.

Meanwhile, for the angle of -80.74° predicted for the onset of mode II crack growth, no observations were found in literature. The SEM observations of Asp et al. in [51] focused on the area ahead of the crack tip, where they found that cracks have an angle of approximately 45° with the horizontal. However, Asp et al. did not observe the first crack formed, closer to the initial crack tip, or its angle. Once more, in-situ mode II delamination tests would be necessary in order to observe the angle of the first crack.

In order to circumvent the necessity of in-situ mode II delamination tests, rail shear tests were performed according to the description in Section 5.3 of the present work. The idea is to qualitatively compare the results of crack-tip angle and onset of cracking

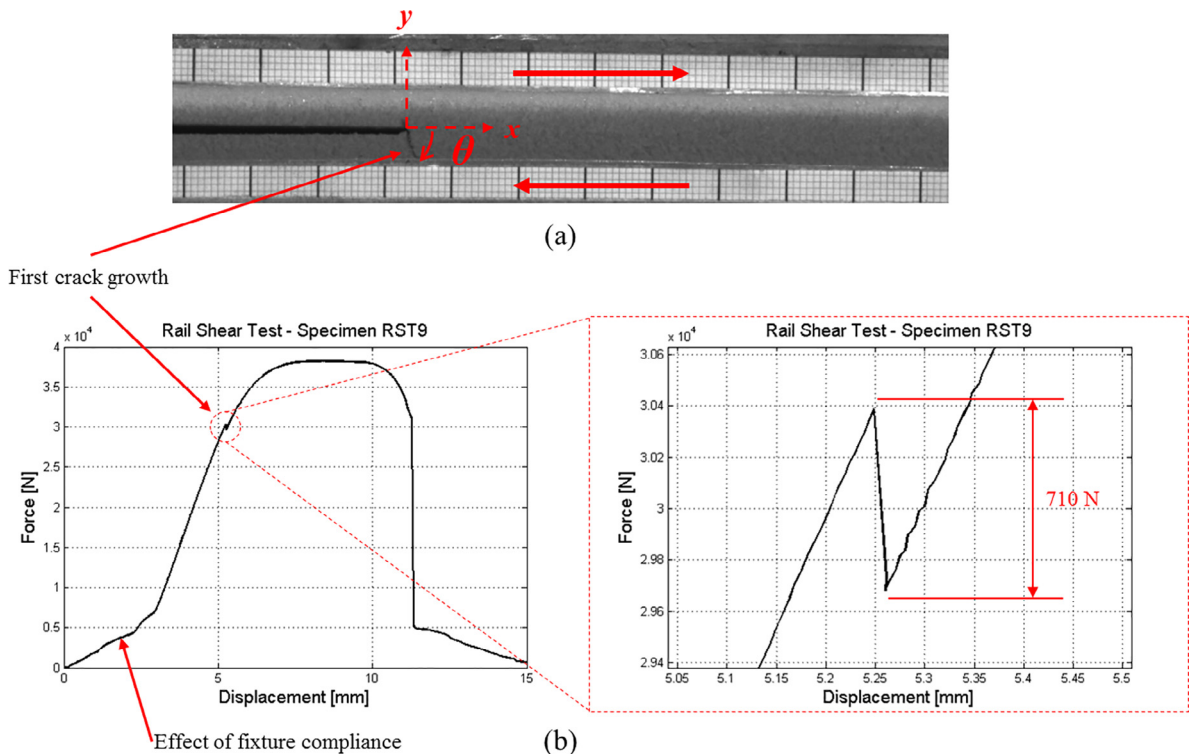


Fig. 7. Specimen RST9: (a) first crack occurs at $\theta = 71^\circ$; (b) a load drop of 710 N is observed when the first crack occurs.

for both rail shear tests and the HTA/6376C carbon/epoxy composite.

Considering the properties of the isotropic foam used in the rail shear tests and approximating the test as yielding a pure mode II loading on the crack tip, Eq. (17) predicts a first crack at an angle of approximately 90° with the x -axis.

The results presented in Fig. 7 show that the first crack in the rail shear sample does occur before the maximum load, such as predicted via the critical SED for composite delamination. In addition, a small load drop is observed, highlighted in Fig. 7(b), at the moment the first crack occurs. This load drop is small (710 N) when compared to the load range of the test (maximum load of approximately 37.5 kN). When scaling this load drop down to the case of delamination in a carbon/epoxy composite, it might not be observed, once the drop in the load is likely to be within the error of the load cell. Besides, the load drop of 710 N was only observed in rail shear specimens when the sampling rate of the testing machine was set to acquire one data point every 0.009 s. When acquiring data points at longer time intervals, the load drop was not obvious.

Given the qualitative similarities between the PVC foam rail shear tests and mode II delamination growth of composites, the rail shear test results indicate that the onset of cracking in mode II delaminations occur, indeed, before the maximum load of the test and before $(G_{IIcr})_{ENF}$.

The angle of the first crack with the x -axis in the rail shear test is of 71° , smaller than the value of 90° predicted by the critical SED approach. This occurs because of the presence of a mode I component at the crack tip in the foam test, which tends to decrease the angle of the crack with the x -axis. This mode I component is inherent to the rail shear test, as described by the ASTM standard [35], and it tends to increase with damage propagation. This increase in the mode I component with damage growth can be observed in the increased crack opening displacement when damage has developed, shown in detail in Fig. 8.

Further in the rail shear test, cracks develop ahead of the main crack tip, and a typical cusp formation can be observed in Fig. 9. The reader should note that the angle of the cracks ahead of the main crack tip is smaller than the angle of the first crack, as listed in Table 6 for every rail shear specimen tested. This is in qualitative agreement with the observations of Asp et al. [51] in which the cracks ahead of the crack tip have an angle of 45° (see Fig. 6), while the critical SED approach predicts the first crack to be at an angle of -80.74° .

The critical SED approach predicted the onset of mode II delamination growth to occur at 23% of $(G_{IIcr})_{ENF}$, which is approximately 50% of the critical load obtained on the ENF test. Meanwhile, the onset of crack growth in the rail shear tests occurred, on average, at 68% of the critical load. Asp et al. observed cracks ahead of the main crack tip at an angle of approximately 45° with the x -axis, while the rail shear tests yielded cracks ahead of the main crack tip with angles between 39° and 69° .

In addition, no load drops are reported in literature before the maximum load in mode II delamination tests, when the first crack growth is predicted to occur by the critical SED approach. In rail shear tests, a small load drop, considering the load range of the test, was observed when the first crack growth occurred. However, due to this load drop being very small and captured only with a high sampling rate, it is reasonable to assert that it is not observed on carbon/epoxy composite specimens in ENF tests when the onset of delamination growth occurs.

Quantitatively, the results of the rail shear tests do not match perfectly the results of the mode II delamination tests. This is expected, since the rail shear test is only a qualitative approximation to pure mode II ply delamination. From the qualitative perspective, the similarities between pure mode II ply delamination and the rail shear tests of the PVC foam are undeniable. Both show the formation of a process zone ahead of the crack tip, with cracks with a less steep angle with the x -axis than the angle of the first crack predicted by the critical SED approach. Therefore, the SED approach seems to yield valid results for the prediction of the first crack growth in mode II delaminations. Furthermore, this prediction was done using only material properties and mode I fracture toughness data.

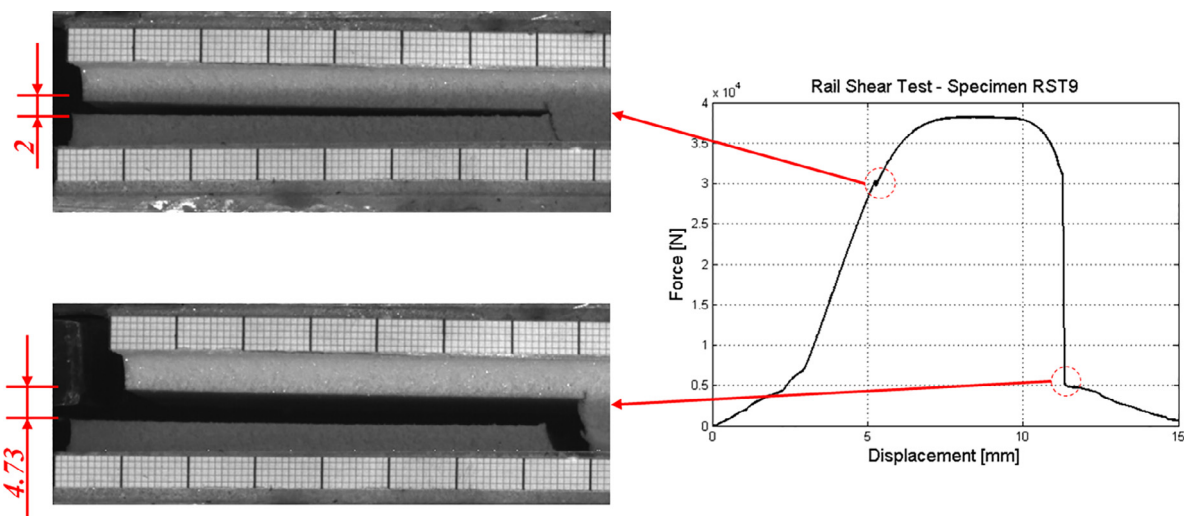


Fig. 8. Specimen RST9: Pictures of the test show influence of mode I component in the test.

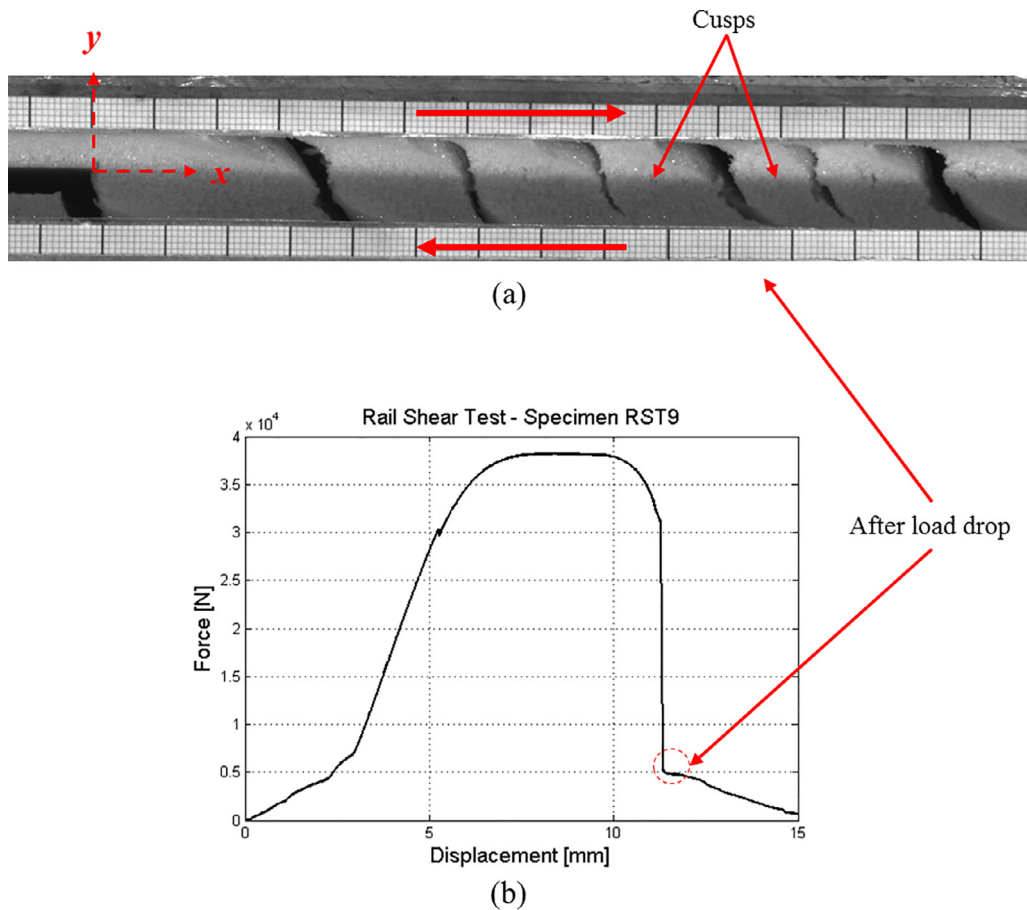


Fig. 9. (a) Cusps formation after coalescence; (b) load-displacement curve – point after cusps coalescence indicated by red arrow.

Table 6

Rail Shear test results; θ_0 is the angle of the first crack relative to the x-axis.

	θ_0	Cusp angles range	$\frac{P_{onset}}{P_{maximum}}$
RST 8	68°	44–55°	0.59
RST 9	71°	54–69°	0.79
RST 10	62°	46–56°	0.67
RST 11	66°	39–56°	0.68

However, what is the use of predicting that the first cracking starts at approximately 23% of $(G_{IIcr})_{ENF}$ for mode II delaminations?

A first crack occurring for mode II delaminations at 23% of $(G_{IIcr})_{ENF}$ implies that composite laminates designed using $(G_{IIcr})_{ENF}$ as a basis for quasi-static mode II delamination resistance might have developed defects ahead of the crack tip although operating at SERR levels below $(G_{IIcr})_{ENF}$. In this case, the growth of mode II fatigue cracks is also expected to be faster, since the starting point for the fatigue crack is a laminate in which damage has already developed in the process zone if the structure operated above $(G_{IIcr})_{SED}$. Besides, the critical SED approach supplies the designer with a load or SERR level below which, quasi-statically, there is no damage

Table 7

Predicted critical SERR for the onset of mode II delamination – other composite material systems.

Composite system	G_{Icr}	$(G_{IIcr})_{ENF}$	$(G_{IIcr})_{SED}$	$\frac{(G_{IIcr})_{SED}}{(G_{IIcr})_{ENF}}$	Reference
IM7/8552	200 J/m ²	800 J/m ²	195 J/m ²	0.24	[54]
G40-800/5260	240 J/m ²	900 J/m ²	237 J/m ²	0.26	[54]
AS4/3501-6	220 J/m ²	650 J/m ²	216 J/m ²	0.33	[54]
Glass/LY556	165 J/m ²	1500 J/m ²	157 J/m ²	0.10	[54]

created ahead of the crack tip. This is an important threshold not only for design purposes, but also for performing compliance calibration tests in ENF specimens prior to fracture testing them. If the SERR level is maintained below $(G_{II_{cr}})_{SED}$, the engineer is certain that the compliance calibration procedure did not generate damage ahead of the crack tip. Following the present results, the future studies should aim at validating experimentally $(G_{II_{cr}})_{SED}$ through in-situ experiments and evaluating whether $(G_{II_{cr}})_{SED}$ also works as a threshold for fatigue crack growth.

5.2.2. Other composite material systems

The critical SED approach was also applied to other orthotropic composite laminates for which data is found in literature. The results, listed in Table 7, show that the onset of pure mode II delamination growth seems to occur consistently between 24% and 33% of $(G_{II_{cr}})_{ENF}$ for carbon/epoxy composite systems. Finally, data for one glass/epoxy composite system was also used, and $(G_{II_{cr}})_{SED}$ was determined as approximately 10% of $(G_{II_{cr}})_{ENF}$.

The reader should note that the results shown in Table 7 are for unidirectional specimens. In case of different lay-ups, the critical SED for onset of fracture will change, because the effective material properties also change (e.g., see Eq. (24)). Although the onset of delamination is a matrix dominated failure, the SED in the vicinity of the crack tip is the contribution of how the load was distributed from its application points to the crack tip. This load distribution changes once the effective properties of the laminate change.

The critical SED approach enables the estimation of the critical SERR for the onset of pure mode II delamination growth without the necessity of performing ENF fracture toughness tests. In addition, the author understands that for engineering purposes and in order to comply with standards, it is of interest to determine $(G_{II_{cr}})_{ENF}$. Thus, a first estimation of $(G_{II_{cr}})_{ENF}$ is possible, once $(G_{II_{cr}})_{SED}$ seems to be approximately 25% of $(G_{II_{cr}})_{ENF}$ for carbon/epoxy composite systems with a toughened matrix. This is the case for IM7/8552, G40-800/5260 and HTA/6376C. For AS4/3501-6, a carbon/epoxy composite with a brittle matrix, $(G_{II_{cr}})_{SED}$ is 33% of $(G_{II_{cr}})_{ENF}$.

The exact value of $(G_{II_{cr}})_{SED}/(G_{II_{cr}})_{ENF}$ depends on how much the microcracks in the process zone will extend before coalescence is reached. The tougher the resin, the longer will be the process zone and coalescence will be reached much after the occurrence of the first crack [13,14], decreasing $(G_{II_{cr}})_{SED}/(G_{II_{cr}})_{ENF}$. This explains the variation of $(G_{II_{cr}})_{SED}/(G_{II_{cr}})_{ENF}$ from 0.23 to 0.33 for the carbon/epoxy composites.

For the glass/epoxy composite system Glass/LY556, the value of $(G_{II_{cr}})_{SED}/(G_{II_{cr}})_{ENF}$ decreases to 0.10 because glass fibres are less stiff than carbon fibres. Due to this reduced stiffness of the glass fibres, the constraint to shear deformation in the resin is smaller. Because of this, the process zone increases in volume, causing coalescence to occur later [13,14] and explaining $(G_{II_{cr}})_{SED}/(G_{II_{cr}})_{ENF} = 0.10$ for Glass/LY556.

Therefore, the relationship between $(G_{II_{cr}})_{SED}$ and $(G_{II_{cr}})_{ENF}$ can be explained by the material properties of the composite systems studied. The exact nature and form of this relationship between material properties and the difference between $(G_{II_{cr}})_{SED}$ and $(G_{II_{cr}})_{ENF}$ is yet to be investigated in future studies. However, the fact that a relationship based on material properties between $(G_{II_{cr}})_{SED}$ and $(G_{II_{cr}})_{ENF}$ exists indicates that the fracture behaviour of the material can be fully characterized with the critical SED approach, performing only mode I fracture toughness tests and having the material properties.

The process to fully characterize the fracture behaviour of the material with the SED approach is illustrated in Fig. 10. Fig. 10(a) shows the current procedure to characterize delamination growth, which involves DCB, ENF and MMB tests. Meanwhile, Fig. 10(b)

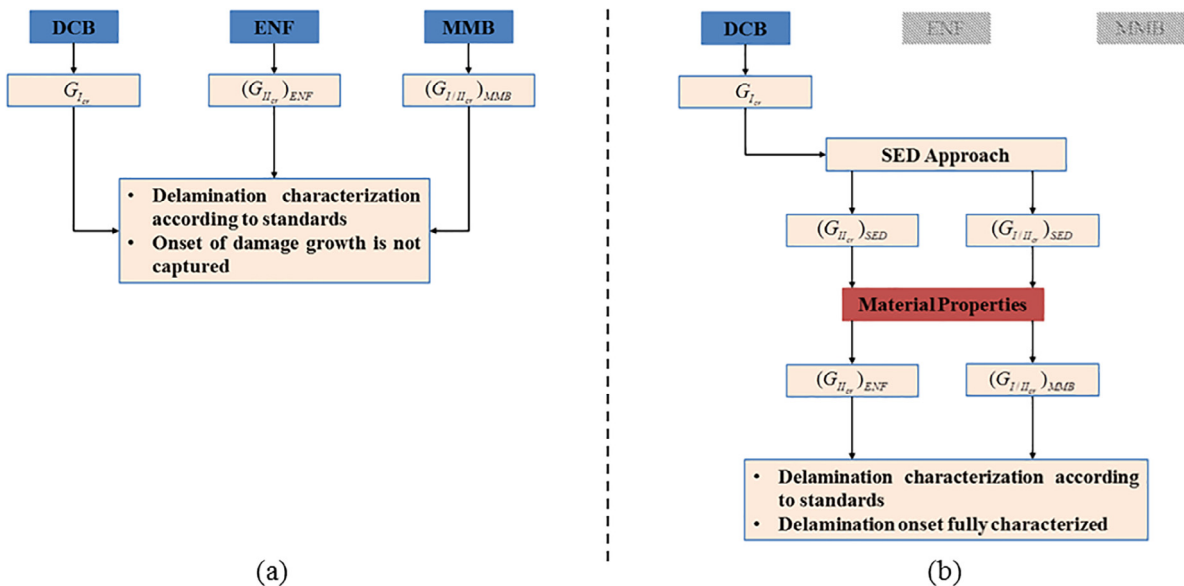


Fig. 10. Flowchart of the (a) current procedure to characterize fracture; and (b) SED approach – ENF and Mixed-Mode Bending (MMB) tests might not be necessary for fracture characterization.

shows the SED approach, for which only DCB fracture tests are necessary in order to characterize delamination onset. Until the moment when $(G_{II_{cr}})_{SED}$ and $(G_{I/II_{cr}})_{SED}$ are obtained, only physics-based relationships are used to obtain the prediction. However, due to engineering purposes, as discussed above, it is interesting to obtain the critical SERR as measured by ENF and MMB tests. To this aim, data from literature and material properties show a relationship between the SERR obtained via the SED approach and the one obtained via standardized tests. However, the exact mathematical form of this relationship is not clear to the present moment.

The characterization of mixed-mode fracture follows the same approach, depicted in Eqs. (25) and (26) where $S_{I/II_{cr}}$ is the critical SED for mixed-mode fracture at a certain mode mixity. This topic will have to be addressed in detail in future publications.

$$S_{I_{cr}} = S_{I/II_{cr}} \tag{25}$$

$$S_{I_{cr}} = K_I^2 D_1 + K_{II}^2 D_2 + K_I K_{II} D_3 \tag{26}$$

5.3. The fundamental relationship between pure mode I and pure mode II crack growth

The SED necessary for a material to fracture is constant, independently of the loading mode. This hypothesis results on Eq. (18) and seems to be validated by the ability to predict pure mode II SIF or SERR based only on material properties and pure mode I fracture toughness data.

Eq. (18) gives a physics-based relationship between mode I and mode II fracture. The critical SED is equal for both loading modes. Therefore, mode I and mode II fracture are intrinsically related. Furthermore, mode I and mode II SIF relate to each other according to the manner the stresses distribute around the crack tip. Using Eq. (18) as a starting point, for linear elastic, isotropic materials, one obtains Eq. (19). Similarly, for linear elastic, orthotropic materials, using Eq. (18) as a starting point, one obtains Eq. (23). Both Eqs. (19) and (23) show that the ratio between mode II and mode I SIF (or SERR) is given by functions that determine how the stresses and, hence, the strain energy, are distributed around the crack tip for each loading mode.

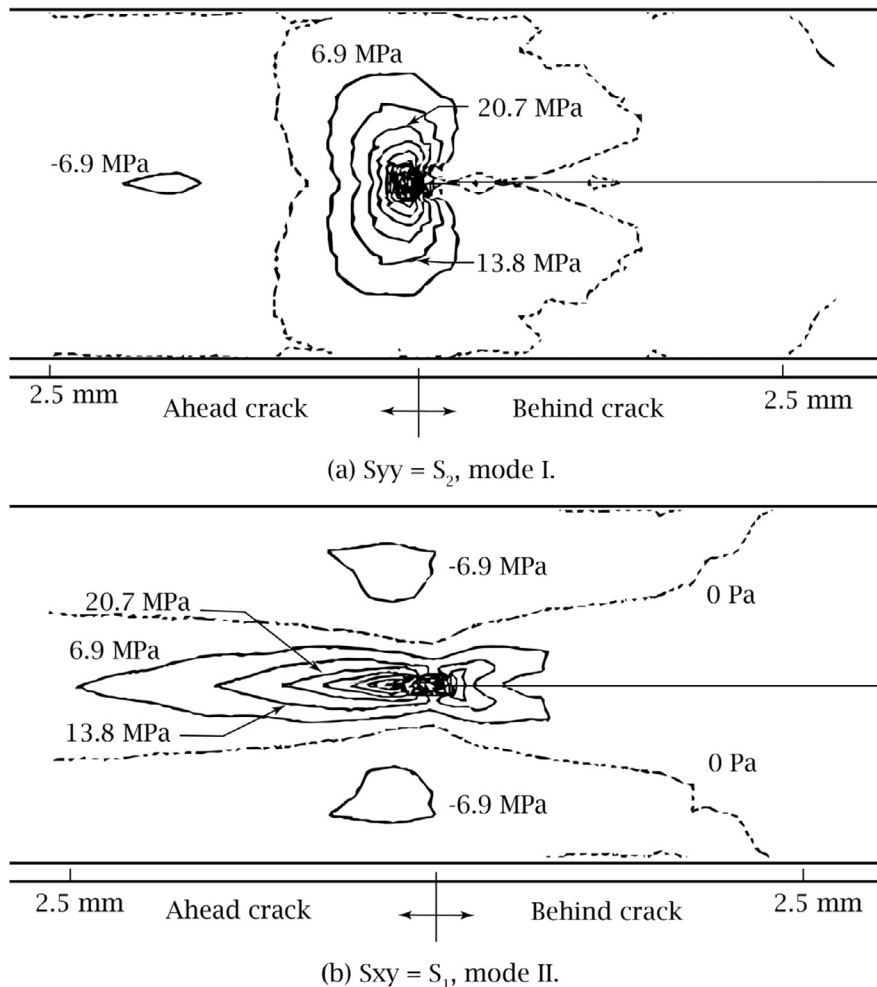


Fig. 11. Comparison on stress distributions around the crack tip for (a) pure mode I and (b) pure mode II delamination (adapted from [15]).

This is shown in Eq. (27), where $D_1(\theta_{0I})$ is the stress distribution function for pure mode I delamination and $D_2(\theta_{0II})$ is the stress distribution function for pure mode II delamination. Eq. (27) gives an insight on why the SERR for the onset of a mode I crack is actually higher than the SERR for the onset of a mode II crack in an orthotropic composite structure: because of the way the stresses are distributed in the vicinity of the crack tip.

$$\frac{G_{IIcr}}{G_{Icr}} = \frac{F_{II} D_1(\theta_{0I})}{F_I D_2(\theta_{0II})} \tag{27}$$

On two different studies, Corleto and Bradley performed finite element simulations in order to understand the differences on the stress distribution of pure mode I and pure mode II delaminations of orthotropic carbon/epoxy specimens [15,16]. The results of their analyses are reproduced, for convenience of the reader, in Fig. 11.

Although the stress levels for both mode I and mode II delamination are very similar, the stress distribution in pure mode II delamination extends for a longer distance in the x-axis than for mode I delaminations, as seen in Fig. 11. This difference in stress distribution ahead of the crack tip is responsible for the difference in damage mechanisms observed on the fracture surfaces of the specimens, as discussed in [52]. For example, the shear stresses in pure mode II delaminations extend for a longer length, and this explains the large process zone typically encountered on shear delaminations. This process zone gives rise to cusps [52].

The way the stress distributes around the crack tip indicates which damage mechanisms will act in fracture. This gives a hint on why previous studies were not able to relate modes I and II SIF or SERR on a physics-based theory until the present moment: because the SIF or the SERR alone do not completely describe the physics of fracture! This is exemplified in Fig. 12 for crack tip stresses in the x-direction. The damage mechanisms acting in fracture are a core part of the crack growth process, and changes in damage mechanisms lead to changes in energy dissipation in crack growth [12,52]. Therefore, the complete stress functions, with the SIF and the functions that describe the stress distribution, must be used to characterize energy dissipation in fracture.

Furthermore, the SIF is a scalar, in an attempt to describe the stress field. With a change in the stress field, the magnitude of the SIF will change. However, how does this change in magnitude of the SIF completely describe the stress field? Hypothetically, one could have two stress fields with a different SIF, but with the same strain energy density in that volume. So, if one wants to relate this change in stress field with a change in the strain energy, this is not possible through the SIF or the SERR alone. The manner of considering the complete stress functions and the contribution of stresses in all directions is through the strain energy density function.

Consider the example of changing the mode of loading for the same material. In this case, the SIF will change. However, the damage mechanisms will also change, and this is accounted for by a change in the functions that say how the stresses distribute in the vicinity of the crack tip, f_1 and f_2 in Fig. 12, such that the SED will remain constant. This means that the leading parameter in crack initiation is the contribution of the SIF (or SERR) together with the stress functions: the SED is the parameter leading crack initiation!

6. Conclusions

The critical SED approach was proposed for the analysis of fracture propagation in different brittle materials. The onset of crack

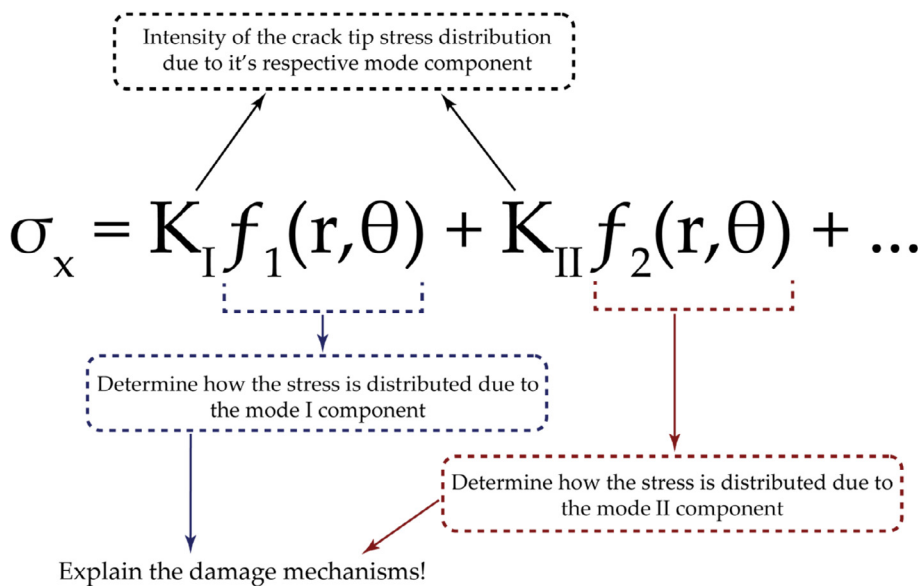


Fig. 12. Crack-tip stresses in x-direction under a mixed-mode loading. The whole stress function is necessary in order to properly characterize fracture. The stress distribution determines the damage mechanisms activated in fracture. Although only the stresses in x-direction are shown for simplicity, note that stresses in 3 directions are used in the SED approach.

growth occurs when the strain energy density in the vicinity of the crack tip reaches a critical value. This critical SED for the onset of crack growth is constant, independently of the loading mode, and it gives a physics-based relationship between the different loading modes. The past attempts to relate fracture under different loading modes using the SIF or the SERR failed because these terms are not sufficient to describe the fracture behaviour. The damage mechanisms acting in fracture are a core part of the crack growth process, and changes in damage mechanisms lead to changes in energy dissipation in crack growth. Therefore, the complete stress functions, with the SIF and the functions that describe the stress distribution, must be used to characterize energy dissipation in fracture. The manner of considering the complete stress functions and the contribution of stresses in all directions is through the strain energy density function.

For delamination of composites, mode II fracture toughness, obtained via standardized tests such as the ENF, does not represent the onset of delamination growth. Instead, the mode II SERR measured with the ENF test refers to the point where the microcracks ahead of the main crack tip coalesce. This explains why mode II fracture toughness is reported in literature to be higher than mode I fracture toughness for delamination of composites. Mode II fracture toughness for the actual onset of delamination growth is smaller than mode I fracture toughness for the onset of growth, and can be obtained via the critical SED approach. The SERR for the onset of mode II delamination growth can be used as a threshold for the development of damage in laminated structures under interlaminar shear quasi-static loading.

Furthermore, using the critical SED approach, only material properties and mode I fracture toughness tests are necessary to characterize the delamination behaviour of a composite structure. The SERR for the onset of delamination growth can then be estimated and potentially used as a threshold for the development of damage under quasi-static loading conditions. In addition, using the material properties, the SERR for the onset of delamination growth can be related with the SERR determined via standardized ENF tests.

Appendix A

The complete deduction of the crack tip stresses and SED function for isotropic and orthotropic materials is presented hereafter.

Consider a structure made of an isotropic, linear elastic material under a general three-dimensional stress state. The strain energy stored in an element of volume dV is given by Eq. (A1), where $G = E/2(1 + \nu)$ is the shear modulus, E is the elastic modulus and ν is Poisson's ratio [36].

$$dW = \left[\frac{1}{2E}(\sigma_x^2 + \sigma_y^2 + \sigma_z^2) - \frac{\nu}{E}(\sigma_x\sigma_y + \sigma_y\sigma_z + \sigma_z\sigma_x) + \frac{1}{2G}(\tau_{xy}^2 + \tau_{xz}^2 + \tau_{yz}^2) \right] dV \tag{A1}$$

Suppose that this structure has a through-crack that extends in the xz -plane, illustrated in Fig. 3. The stresses around the crack tip were described by Irwin [37] and are given by

$$\begin{aligned} \sigma_x &= \frac{K_I}{\sqrt{2\pi r}} \cos(\theta/2) [1 - \sin(\theta/2)\sin(3\theta/2)] - \frac{K_{II}}{\sqrt{2\pi r}} \sin(\theta/2) [2 + \cos(\theta/2)\cos(3\theta/2)] \\ \sigma_y &= \frac{K_I}{\sqrt{2\pi r}} \cos(\theta/2) [1 + \sin(\theta/2)\sin(3\theta/2)] + \frac{K_{II}}{\sqrt{2\pi r}} \sin(\theta/2) \cos(\theta/2) \cos(3\theta/2) \\ \sigma_z &= 2\nu \frac{K_I}{\sqrt{2\pi r}} \cos(\theta/2) - 2\nu \frac{K_{II}}{\sqrt{2\pi r}} \sin(\theta/2) \\ \tau_{xy} &= \frac{K_I}{\sqrt{2\pi r}} \cos(\theta/2) \sin(\theta/2) \cos(3\theta/2) + \frac{K_{II}}{\sqrt{2\pi r}} \cos(\theta/2) [1 - \sin(\theta/2)\sin(3\theta/2)] \end{aligned} \tag{A2}$$

with higher order terms in r neglected. K_i stands for the Stress Intensity Factor (SIF), being i the loading mode (I, II or III).

Substituting the stresses given by Eq. (A2) in Eq. (A1), one obtains the strain energy stored in a volume element dV at any point around the crack tip, which is

$$\frac{dW}{dV} = \frac{1}{\pi r} (a_{11}K_I^2 + 2a_{12}K_IK_{II} + a_{22}K_{II}^2) \tag{A3}$$

The intensity of the strain energy density field around the crack tip is, then, given by

$$S = a_{11}K_I^2 + 2a_{12}K_IK_{II} + a_{22}K_{II}^2 \tag{A4}$$

where the coefficients a_{11} , a_{12} and a_{22} are given by

$$\begin{aligned} a_{11} &= \frac{1}{16G} [(3 - 4\nu - \cos\theta)(1 + \cos\theta)] \\ a_{12} &= \frac{1}{16G} 2\sin\theta [\cos\theta - (1 - 2\nu)] \\ a_{22} &= \frac{1}{16G} [4(1 - \nu)(1 - \cos\theta) + (1 + \cos\theta)(3\cos\theta - 1)] \end{aligned} \tag{A5}$$

For the cases of pure mode I and pure mode II loading, the SED is given by respectively

$$S_I = \frac{K_I^2}{16G} [(3 - 4\nu - \cos\theta)(1 + \cos\theta)] \tag{A6}$$

$$S_{II} = \frac{K_{II}^2}{16G} [4(1 - \nu)(1 - \cos\theta) + (1 + \cos\theta)(3\cos\theta - 1)] \tag{A7}$$

A.1. Orthotropic materials

Consider, once more, a structure with a through-crack that extends on the xz -plane, shown in Fig. 3. This time the structure is made of a linear elastic, orthotropic material. In this case, the strain energy stored in a volume element dV is

$$\frac{dW}{dV} = \frac{1}{2} \left[\frac{\sigma_x^2}{E_x} + \frac{\sigma_y^2}{E_y} + \frac{\sigma_z^2}{E_z} + \frac{\tau_{xy}^2}{G_{xy}} \right] - \frac{\nu_{xy}\sigma_x\sigma_y}{E_x} - \frac{\nu_{xz}\sigma_x\sigma_z}{E_x} - \frac{\nu_{yz}\sigma_y\sigma_z}{E_y} \tag{A8}$$

The stresses around the crack tip of orthotropic bodies were described by Sih et al. [38] and are given in the expressions in

$$\begin{aligned} \sigma_x &= \frac{K_I}{\sqrt{2\pi r}} A_I + \frac{K_{II}}{\sqrt{2\pi r}} A_{II} \\ \sigma_y &= \frac{K_I}{\sqrt{2\pi r}} B_I + \frac{K_{II}}{\sqrt{2\pi r}} B_{II} \\ \sigma_z &= \left(\frac{K_I}{\sqrt{2\pi r}} A_I + \frac{K_{II}}{\sqrt{2\pi r}} A_{II} \right) \frac{\nu_{xz} E_z}{E_x} + \left(\frac{K_I}{\sqrt{2\pi r}} B_I + \frac{K_{II}}{\sqrt{2\pi r}} B_{II} \right) \frac{\nu_{yz} E_z}{E_y} \\ \tau_{xy} &= \frac{K_I}{\sqrt{2\pi r}} C_I + \frac{K_{II}}{\sqrt{2\pi r}} C_{II} \end{aligned} \tag{A9}$$

The coefficients A_i , B_i and C_i , for $i = I$ and II , are given in

$$\begin{aligned} A_I &= \operatorname{Re} \left\{ \frac{\mu_1 \mu_2}{\mu_1 - \mu_2} \left(\frac{\mu_2}{\sqrt{\cos\theta + \mu_2 \sin\theta}} - \frac{\mu_1}{\sqrt{\cos\theta + \mu_1 \sin\theta}} \right) \right\} \\ A_{II} &= \operatorname{Re} \left\{ \frac{1}{\mu_1 - \mu_2} \left(\frac{\mu_2^2}{\sqrt{\cos\theta + \mu_2 \sin\theta}} - \frac{\mu_1^2}{\sqrt{\cos\theta + \mu_1 \sin\theta}} \right) \right\} \\ B_I &= \operatorname{Re} \left\{ \frac{1}{\mu_1 - \mu_2} \left(\frac{\mu_1}{\sqrt{\cos\theta + \mu_2 \sin\theta}} - \frac{\mu_2}{\sqrt{\cos\theta + \mu_1 \sin\theta}} \right) \right\} \\ B_{II} &= \operatorname{Re} \left\{ \frac{1}{\mu_1 - \mu_2} \left(\frac{1}{\sqrt{\cos\theta + \mu_2 \sin\theta}} - \frac{1}{\sqrt{\cos\theta + \mu_1 \sin\theta}} \right) \right\} \\ C_I &= \operatorname{Re} \left\{ \frac{\mu_1 \mu_2}{\mu_1 - \mu_2} \left(\frac{1}{\sqrt{\cos\theta + \mu_1 \sin\theta}} - \frac{1}{\sqrt{\cos\theta + \mu_2 \sin\theta}} \right) \right\} \\ C_{II} &= \operatorname{Re} \left\{ \frac{1}{\mu_1 - \mu_2} \left(\frac{\mu_1}{\sqrt{\cos\theta + \mu_1 \sin\theta}} - \frac{\mu_2}{\sqrt{\cos\theta + \mu_2 \sin\theta}} \right) \right\} \end{aligned} \tag{A10}$$

μ_1 and μ_2 are obtained from each of the conjugate pair of roots of $A_{11}\mu^4 + (2A_{12} + A_{66})\mu^2 + A_{22} = 0$, where the coefficients A_{11} , A_{12} , A_{22} and A_{66} are obtained from the stress-strain relationships in [39]

$$\begin{aligned} \epsilon_x &= A_{11}\sigma_x + A_{12}\sigma_y + A_{13}\sigma_z + A_{16}\tau_{xy} \\ \epsilon_y &= A_{21}\sigma_x + A_{22}\sigma_y + A_{23}\sigma_z + A_{26}\tau_{xy} \\ \epsilon_z &= A_{61}\sigma_x + A_{62}\sigma_y + A_{63}\sigma_z + A_{66}\tau_{xy} \end{aligned} \tag{A11}$$

Substituting the stresses from Eq. (A9) in Eq. (A8), one obtains

$$\frac{dW}{dV}(\theta) = \frac{1}{2\pi r} (K_I^2 D_1 + K_{II}^2 D_2 + K_I K_{II} D_3) \tag{A12}$$

Where the SED is $S = K_I^2 D_1 + K_{II}^2 D_2 + K_I K_{II} D_3$ and the coefficients D_i , for $i = 1, 2$ and 3 , are given by

$$\begin{aligned} D_1 &= \frac{A_I^2}{2E_x} + \frac{B_I^2}{2E_y} + \frac{C_I^2}{2G_{xy}} - \frac{A_I B_I \nu_{xy}}{E_x} - \frac{A_I^2 \nu_{xz}^2 E_z}{2E_x^2} - \frac{B_I^2 \nu_{yz}^2 E_z}{2E_y^2} - \frac{A_I B_I \nu_{xz} \nu_{yz} E_z}{E_x E_y} \\ D_2 &= \frac{A_{II}^2}{2E_x} + \frac{B_{II}^2}{2E_y} + \frac{C_{II}^2}{2G_{xy}} - \frac{A_{II} B_{II} \nu_{xy}}{E_x} - \frac{A_{II}^2 \nu_{xz}^2 E_z}{2E_x^2} - \frac{B_{II}^2 \nu_{yz}^2 E_z}{2E_y^2} - \frac{A_{II} B_{II} \nu_{xz} \nu_{yz} E_z}{E_x E_y} \\ D_3 &= \frac{A_I A_{II}}{E_x} + \frac{B_I B_{II}}{E_y} + \frac{C_I C_{II}}{G_{xy}} - \frac{A_I B_{II} \nu_{xy}}{E_x} - \frac{A_{II} B_I \nu_{xy}}{E_x} - \frac{A_I A_{II} \nu_{xz}^2 E_z}{E_x^2} - \frac{B_I B_{II} \nu_{yz}^2 E_z}{E_y^2} - \frac{A_I B_{II} \nu_{xz} \nu_{yz} E_z}{E_x E_y} - \frac{A_{II} B_I \nu_{xz} \nu_{yz} E_z}{E_x E_y} \end{aligned} \tag{A13}$$

For orthotropic materials under plane stress the SERR for both mode I and mode II loading are [39]

$$\begin{aligned} G_I &= F_I K_I^2 \\ G_{II} &= F_{II} K_{II}^2 \end{aligned} \tag{A14}$$

Where

$$F_I = \sqrt{\frac{A_{11} A_{22}}{2}} \left[\sqrt{\frac{A_{22}}{A_{11}}} + \frac{2A_{12} + A_{66}}{2A_{11}} \right]^{1/2} \tag{A15}$$

$$F_{II} = \frac{A_{11}}{\sqrt{2}} \left[\sqrt{\frac{A_{22}}{A_{11}}} + \frac{2A_{12} + A_{66}}{2A_{11}} \right]^{1/2} \tag{A16}$$

And the coefficients A_{11} , A_{12} , A_{22} and A_{66} are given in Eq. (A11). Under plane strain conditions, Eqs. (A15) and (A16) should be used with the following substitution

$$A_{ij} = A_{ij} - \frac{A_{i3}A_{j3}}{A_{33}} \quad (\text{A17})$$

References

- [1] Khan R. Delamination growth in composites under fatigue loading [PhD Thesis] Delft: Delft University of Technology; 2013.
- [2] Hojo M, Ando T, Tanaka M, Adachi T, Ochiai S, Endo Y. Modes I and II interlaminar fracture toughness and fatigue delamination of CF/epoxy laminates with self-same epoxy interleaf. *Int J Fatigue* 2006;28:1154–65.
- [3] Hojo M, Ochiai S, Gustafson C-G, Tanaka K. Effect of matrix resin on delamination fatigue crack growth in CFRP laminates. *Eng Fract Mech* 1994;49:35–47.
- [4] Pascoe JA, Alderliesten RC, Benedictus R. Methods for the prediction of fatigue delamination growth in composites and adhesive bonds - a critical review. *Eng Fract Mech* 2013;112–113:72–96.
- [5] Jones R, Kinloch AJ, Hu W. Cyclic-fatigue crack growth in composite and adhesively-bonded structures: the FAA slow crack growth approach to certification and the problem of similitude. *Int J Fatigue* 2016;88:10–8.
- [6] Jones R, Kinloch A, Michopoulos J, Brunner AJ, Phan N. Delamination growth in polymer-matrix fibre composites and the use of fracture mechanics data for material characterisation and life prediction. *Compos Struct* 2017.
- [7] Amaral L, Alderliesten R, Benedictus R. Understanding mixed-mode cyclic fatigue delamination growth in unidirectional composites: an experimental approach. *Eng Fract Mech* 2017;180:161–78.
- [8] Jones R, Stelzer S, Brunner AJ. Mode I, II and Mixed Mode I/II delamination growth in composites. *Compos Struct* 2014;110:317–24.
- [9] ASTM Standard D5528-01. Standard Test Method for Mode I Interlaminar Fracture Toughness of Unidirectional Fiber-Reinforced Polymer Matrix Composites. US: ASTM International; 2007.
- [10] Amaral L, Yao L, Alderliesten R, Benedictus R. The relation between the strain energy release in fatigue and quasi-static crack growth. *Eng Fract Mech* 2015;145:86–97.
- [11] Amaral L, Yao L, Alderliesten RC, Benedictus R. Energy based study on quasi-static delamination growth treated as a low cycle fatigue process. In: Siljander A, editor. 34th Conference and 28th Symposium of the International Committee on Aeronautical Fatigue and Structural Integrity. Helsinki, Finland; 2015. p. 240–8.
- [12] Amaral L, Zarouchas D, Alderliesten R, Benedictus R. Energy dissipation in mode II fatigue crack growth. *Eng Fract Mech* 2017;173:41–54.
- [13] Bradley WL, Cohen RN. Matrix deformation and fracture in graphite-reinforced epoxies. Delamination and debonding of materials. ASTM International; 1985.
- [14] Hibbs MF, Bradley WL. Correlations between micromechanical failure processes and the delamination toughness of graphite/epoxy systems. In: *Fractography of Modern Engineering Materials: Composites and Metals*. ASTM International; 1987.
- [15] Corleto C, Bradley W, Henriksen M. Correspondence between stress fields and damage zones ahead of crack tip of composites under mode I and mode II delamination. In: International conference on composite materials, 6th, and European conference on composite materials, 2nd, London, England; 1987. p. 3.
- [16] Corleto C, Bradley W. Mode II delamination fracture toughness of unidirectional graphite/epoxy composites. *Compos Mater: Fatigue Fract* 1989;2:201–21.
- [17] Russell AJ. Micromechanisms of interlaminar fracture and fatigue. *Polym Compos* 1987;8:342–51.
- [18] Jordan WM, Bradley WL. Micromechanisms of fracture in toughened graphite-epoxy laminates. *Toughened Composites*. ASTM International; 1987.
- [19] Ayatollahi M, Pavier M, Smith D. Determination of T-stress from finite element analysis for mode I and mixed mode I/II loading. *Int J Fract* 1998;91:283–98.
- [20] Smith D, Ayatollahi M, Pavier M. On the consequences of T-stress in elastic brittle fracture. In: *Proceedings of the Royal Society of London A: Mathematical, Physical and Engineering Sciences*. The Royal Society; 2006. p. 2415–37.
- [21] Ayatollahi M, Hashemi R. Computation of stress intensity factors (KI, KII) and T-stress for cracks reinforced by composite patching. *Compos Struct* 2007;78:602–9.
- [22] Griffith AA. The Phenomena of Rupture and Flow in Solids. *Philos Trans Roy Soc Lond Series A* 1921;221:163–98. Containing Papers of a Mathematical or Physical Character.
- [23] Sih GC. *Mechanics of fracture initiation and propagation: surface and volume energy density applied as failure criterion*. Springer Science & Business Media; 2012.
- [24] Sih G, Macdonald B. Fracture mechanics applied to engineering problems-strain energy density fracture criterion. *Eng Fract Mech* 1974;6:361–86.
- [25] Neuber H. Theory of stress concentration for shear-strained prismatical bodies with arbitrary nonlinear stress-strain law. *J Appl Mech* 1961;28:544–50.
- [26] Neuber H. Theoretical calculation of strength at stress concentration. *Czechoslovak J Phys B*. 1969;19:400–.
- [27] Lazzarin P, Zambardi R. A finite-volume-energy based approach to predict the static and fatigue behavior of components with sharp V-shaped notches. *Int J Fract* 2001;112:275–98.
- [28] Berto F, Lazzarin P. A review of the volume-based strain energy density approach applied to V-notches and welded structures. *Theor Appl Fract Mech* 2009;52:183–94.
- [29] Lee SM. Mode II delamination failure mechanisms of polymer matrix composites. *J Mater Sci* 1997;32:1287–95.
- [30] Lee SM, Mode II. Interlaminar crack growth process in polymer matrix composites. *J Reinf Plast Compos* 1999;18:1254–66.
- [31] Greenhalgh ES. Failure analysis and fractography of polymer composites: Woodhead Publishing Limited; 2009.
- [32] Rogers C, Greenhalgh E, Robinson P. Developing a mode II fracture model for composite laminates; 2008.
- [33] Greenhalgh ES, Rogers C, Robinson P. Fractographic observations on delamination growth and the subsequent migration through the laminate. *Compos Sci Technol* 2009;69:2345–51.
- [34] Divinycell H. grade, Technical Manual. Divinycell International AB; 1991.
- [35] C273 A. 273. Standard Test Method for Shear Properties of Sandwich Core Materials. The American Society for Testing and Materials; 2000.
- [36] Boreisi AP, Schmidt RJ, Sidebottom OM. *Advanced mechanics of materials*: Wiley, New York; 1993.
- [37] Irwin GR. Analysis of stresses and strains near the end of a crack traversing a plate. *ASME J Appl Mech* 1957;24:361–4.
- [38] Sih GC, Paris PC, Irwin GR. On cracks in rectilinearly anisotropic bodies. *Int J FractMech* 1965;1:189–203.
- [39] Tada H, Paris PC, Irwin GR. *The stress analysis of cracks*. Handbook: Del Research Corporation; 1973.
- [40] Erdogan F, Tuncel O, Paris P. An experimental investigation of the crack tip stress intensity factors in plates under cylindrical bending. *ASME J Basic Eng* 1962;84:542–6.
- [41] Erdogan F, Sih G. On the crack extension in plates under plane loading and transverse shear. *J Basic Eng* 1963;85:519–27.
- [42] Wong T-F. Micromechanics of faulting in Westerly granite. *International journal of rock mechanics and mining sciences & geomechanics abstracts*. Elsevier; 1982. p. 49–64.
- [43] Ingraffea AR. Mixed-mode fracture initiation in Indiana limestone and Westerly granite. In: *The 22nd US Symposium on Rock Mechanics (USRMS)*. American Rock Mechanics Association; 1981.
- [44] Daneshy A. Hydraulic fracture propagation in layered formations. *Soc Petrol Eng J* 1978;18:33–41.
- [45] Van Herwijnen A, Gaume J, Bair EH, Reuter B, Birkeland KW, Schweizer J. Estimating the effective elastic modulus and specific fracture energy of snowpack layers from field experiments. *J Glaciol* 2016;62:997–1007.
- [46] Kirchner H, Michot G, Schweizer J. Fracture toughness of snow in shear and tension. *Scr Mater* 2002;46:425–9.

- [47] McClung D. Dry snow slab quasi-brittle fracture initiation and verification from field tests. *J Geophys Res: Earth Surface* 2009;114.
- [48] Backers T. Fracture toughness determination and micromechanics of rock under mode I and mode II loading: Geoforschungszentrum Potsdam; 2005.
- [49] ASTM. Standard Test Method for Determination of the Mode II Interlaminar Fracture Toughness of Unidirectional Fiber-Reinforced Polymer Matrix Composites. D7905/D7905M ASTM International; 2014.
- [50] Asp L. The effects of moisture and temperature on the interlaminar delamination toughness of a carbon/epoxy composite. *Compos Sci Technol* 1998;58:967–77.
- [51] Asp LE, Sjögren A, Greenhalgh ES. Delamination growth and thresholds in a carbon/epoxy composite under fatigue loading. *J Compos Tech Res* 2001;23:55–68.
- [52] Amaral L, Alderliesten R, Benedictus R. Understanding Mixed-Mode Cyclic Fatigue Delamination Growth in unidirectional composites: an experimental approach. *Eng Fract Mech* 2017.
- [53] Khan R, Alderliesten R, Badshaha S. Experimental investigation of the microscopic damage development at mode I fatigue delamination tips in carbon/epoxy laminates; 2016.
- [54] Kaddour A, Hinton M, Smith P, Li S. Mechanical properties and details of composite laminates for the test cases used in the third world-wide failure exercise. *J Compos Mater* 2013;47:2427–42.